Releasable infrared metamaterials

J. A. D'Archangel[a)] and G. D. Boreman
CREOL, The College of Optics and Photonics, University of Central Florida, 4000 Central Florida Blvd., Orlando, Florida 32816

D.J. Shelton
Plasmonics Inc., 12565 Research Parkway, Suite 300, Orlando, Florida 32826

M. B. Sinclair and I. Brener
Sandia National Laboratories, P.O. 5800, Albuquerque, New Mexico 87185

(Received 11 April 2011; accepted 13 August 2011; published 14 September 2011)

Infrared metamaterial arrays containing Au elements immersed in a medium of benzocyclobutene (BCB) were fabricated and selectively etched to produce small square flakes with edge dimensions of approximately 20 μm. Two unit-cell designs were fabricated successfully: one employed crossed-dipole elements while the other utilized square-loop elements (the latter design was symmetric about a Cr ground plane). Infrared spectral reflectivity measurements from collected flakes were compared to infinite-surface simulations in Ansoft HFSS and spectral reflectance measurements of full array samples. Good agreement was found between modeled and experimental resonant behavior when taking into account the proportionality of flakes filling the input aperture of the measurement apparatus. *© 2011 American Vacuum Society*. [DOI: 10.1116/1.3633695]

I. INTRODUCTION

Metamaterials are a class of engineered materials in which the structure, rather than the composition, dominates the electromagnetic response. With resonance attributed to sub-wavelength geometry, traditional frequency selective surface (FSS) filter designs are considered a metamaterials subcategory. Recently, metamaterials have been shown to control spectral properties such as reflection,[1] transmission,[2] and absorption[3] in the infrared. For convenience, metamaterial structures are often fabricated on semiconductor wafers, which is not conducive for applications involving nonplanar surfaces. The motivation for this work was to devise a processing technique to produce a metamaterial-based coating that could cover nonplanar surface areas. One such solution is to fabricate flexible metamaterial arrays; this has been shown for polyimide substrates[4,5] as well as silicon nitride membranes.[6] Our approach here is to create small flakes containing multiple unit cells of FSS-type resonating elements. These particles would be suitable for implementation in a paint if dispersed in an IR-transparent binder. A coating such as this would contain a random placement of flakes, since they could land on either side and in any rotational orientation. Thus, the unit-cell design of the metamaterial must be symmetric about the center plane of the flakes and should also have spectral characteristics that are invariant to in-plane rotations. This article will present the design, fabrication, and testing of such flakes.

II. UNIT-CELL DESIGN AND MODELING

The design and modeling of the metamaterial flakes began with a unit cell, or rather, a single resonant element. The simulations assumed a periodic and infinite lattice of unit cells; this is in contrast to our fabricated result, a collection of finite periodic arrays of unit cell elements. It has been shown that the resonant behavior should not be critically impacted by the finite extent of passive arrays for situations where on the order of 10 by 10 unit cells are contiguous[7–9]; however, it is intuitive that our measured strength of the resonance is affected due the diminished proportion of flakes in the observation area. Thus, the spectral features of an infinite array of unit cells are the baseline for comparison with the measured response of the collected flakes.

Our first metamaterial flake design consisted of an 8 by 8 array of crossed-dipoles, with a unit-cell periodicity of 1.8 μm and a dipole length of 1.4 μm. The crossed-dipole design is expected to have a fundamental resonance when the dipole length is approximately $\lambda/2$ in the immersion medium. This design incorporated a guard ring (ring of dielectric without elements) on the perimeter of each flake. The purpose of the guard ring was to create a final structure with the elements fully encased in BCB. The second design was an 8 by 8 array of square loop elements, with a periodicity of 2 μm and edges 1.7 μm long. The fundamental resonance of the square-loop occurs when the perimeter is approximately λ in the immersion medium. The square-loop design generally has a broader resonance as compared to the crossed-dipole, due to the decreased inter-element spacing.[7] This design was symmetric about a Cr ground plane with a 0.5 μm resonant cavity of BCB and contained no guard ring. The ground plane was made thick enough such that the wavelengths of interest were significantly attenuated (and thus nearly completely reflected). In the resonant cavity, the BCB layer represents a quarter wave layer in the material; thus enhancing the resonance of the array via thin film interference. The overlayer of BCB served merely to protect the elements from processing and thus was made as thin as our process would allow.

Modeling was carried out in Ansoft High Frequency Structure Simulator (HFSS). HFSS computes the electrical behavior of high-frequency structures using the finite

[a)]Electronic mail: darchangel@creol.ucf.edu

Author complimentary copy. Redistribution subject to AIP license or copyright, see http://jvb.aip.org/jvb/copyright.jsp

element method. The results of HFSS assume an infinite array of unit cells and plane wave illumination at a single angle of incidence. The modeling relied on user input geometry and frequency dependent optical material properties derived from ellipsometry.[10] This greatly increases confidence in the simulation, since optical properties and film thickness can be measured directly after each fabrication step and input into the simulation. This is especially critical in the infrared, due to the finite conductivity of metals. For the crossed-dipole design, the unit cell was simulated on a Si wafer (its environment after collection). The unit-cell simulation for the square-loop design only required the upper half of the flake, as the Cr ground plane was assumed to be a perfect electrical conductor.

III. FABRICATION AND TESTING

Large rectangular arrays (~1 cm^2) of unit cells were fabricated on a Si wafer. The arrays were sandwiched in between a sacrificial layer and an etch mask of SiO_2 to facilitate later processing. A side view of the fabrication design for the crossed-dipole flakes is shown in Fig. 1. First, a 150-nm layer of SiO_2 was deposited via electron beam evaporation upon a clean Si wafer. Next, a 250-nm layer of BCB was added via spin coating. Following this, Au crossed-dipole elements (75-nm thick) were added by electron-beam lithography and lift-off. In this step, Au alignment marks were added for later alignment of the etch mask. Next, a second 250-nm coating of BCB was applied. This was followed by a SiO_2 etch mask patterned by electron beam lithography and lift-off. The fabrication design for the square-loop elements symmetric about a ground plane is shown in Fig. 2. Again, a sacrificial layer of 150-nm SiO_2 was deposited upon a clean Si wafer. The first layer of 125 nm BCB was added by spin coating and followed by the first set of 75-nm thick Au square-loop elements, created by electron beam lithography and lift-off. The second coating (575 nm) of BCB was then applied. At this point, a 150-nm Cr ground plane was added by electron beam evaporation. A third layer of 500 nm BCB was added, followed by another layer of Au elements. After this, the final 200-nm layer of BCB was applied. An etch mask of 150-nm thick SiO_2 was patterned by electron beam lithography.

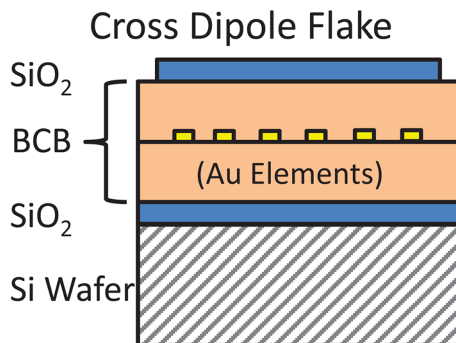

FIG. 1. (Color online) Cross-sectional schematic of the crossed-dipole flake fabrication, showing the wafer substrate, SiO_2 sacrificial layer and etch mask, and Au elements encased in BCB.

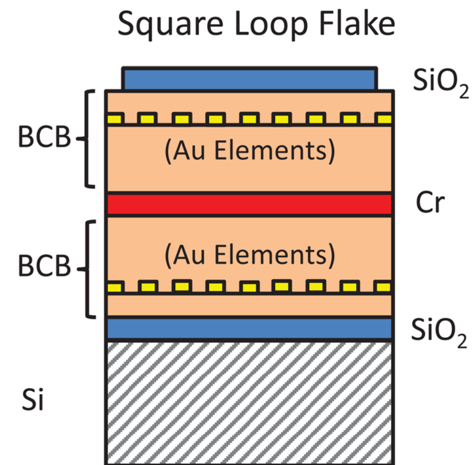

FIG. 2. (Color online) Cross-sectional schematic of the square-loop flake fabrication, showing the wafer substrate, SiO_2 sacrificial layer and etch mask, and two sets of Au elements incased in BCB separated by a Cr ground plane.

For both designs, Au elements were fabricated by direct-write electron beam lithography and liftoff. We used ZEP 520A-7 resist which was cured for 3 min at 180°C. The lithography was performed on a Leica EBPG5000 + electron beam lithography system. The resonant elements had line widths of 200 and 300 nm (square-loop and crossed-dipole, respectively), although the system is capable of much finer resolution.[11] After exposure, the sample was developed in ZEP-RD for 90 s. Au elements were deposited by electron beam evaporation. (A Ti adhesion layer was included before and after each Au deposition). Lift-off was performed in ZEP-remover (N,N-dimethylacetamide) under ultrasonic agitation. The SiO_2 sacrificial layer and etch mask were fabricated using the same equipment and processes as the Au elements. The BCB polymer used in this work was CYCLOTENE 3022-35 (from The Dow Chemical Company). It was chosen due to its tendency toward planarization, previously demonstrated use in FSS at infrared, and in-house fabrication capabilities. In addition, although it exhibits absorption in the 8–13 μm range,[4] BCB is relatively transparent over the wide range of interest. BCB was applied by spin coating, and then hard-cured at 250°C for 5 min on a hot plate, in an inert environment. The fabrication required various thicknesses of BCB. These were realized by mixing BCB with its thinner (mesitylene), and, to a lesser extent, changing the speeds of the spin coater. The thickness of BCB was determined with a J. A. Woollam IR-VASE ellipsometer.

The dimensions of the flakes were defined by the SiO_2 etch mask. The first plasma etch cut through the openings of the etch mask and removed unwanted material down to the ground plane. Next, a wet etch in CHROME ETCH (Ashland Specialty Chemical Company) was used to etch through the Cr ground plane. The final plasma etch cut through the bottom layer of BCB. The plasma etching took place in a Branson P2000 barrel etcher. Etching BCB in this manner requires an introduction of fluorinated gas into the O_2 environment, as O_2 plasma alone is known to lead to a self-passivating etch process.[12] We found that a combination of

Author complimentary copy. Redistribution subject to AIP license or copyright, see http://jvb.aip.org/jvb/copyright.jsp

CF_4 and O_2 that was roughly 1:3 led to etch rates of approximately 150 nm/min at 200 W.

The flakes were released from the substrate in a buffered-oxide etch (BOE), which is known to selectively etch SiO_2. The flakes were released within a few minutes in BOE under ultrasonic agitation, which also removed remaining portions of the etch mask. We found that in the limit of exposure in our experiment, the BOE did not significantly attack the BCB, or for that matter, the Cr. To stop the etching process and collect the flakes, we used a nylon filter screen attached to the end of a syringe. The openings in the filter screen were 11 μm square, roughly half of the intended flake size. The collection of flakes on the filter media were transferred onto a clean Si wafer for observation and testing. The resulting sample was momentarily placed on a 180 °C hot plate to evaporate any remaining BOE. In all observations and measurements, the flakes were merely clinging to the wafer, held slightly by what is believed to be a result of their initially wet application.

The physical results of the fabrication were observed by both optical microscopy and scanning electron microscopy, using an Olympus optical microscope and a Zeiss Ultra-55 scanning electron microscope (SEM). Since the Au metamaterial elements were encased in dielectric, SEM imaging produced images with remarkable contrast. Spectral reflectivity measurements were taken of the collected flakes and also the full array before etching, using a Perkin-Elmer micro-FTIR spectrometer with an input diameter of 100 μm and a full angle field of view of 28°.

IV. RESULTS

The fabricated samples for each flake scheme closely matched our intended designs. Figures 3 and 4 are SEM images of single-flake examples of the crossed-dipole and square-loop designs, respectively. The guard ring contributed to a much cleaner fabrication process, as the presence of elements and the ground plane in between the flakes complicated the BCB removal. The faint perimeter line in Fig. 3 shows a small etch bias from the isotropic plasma etch.

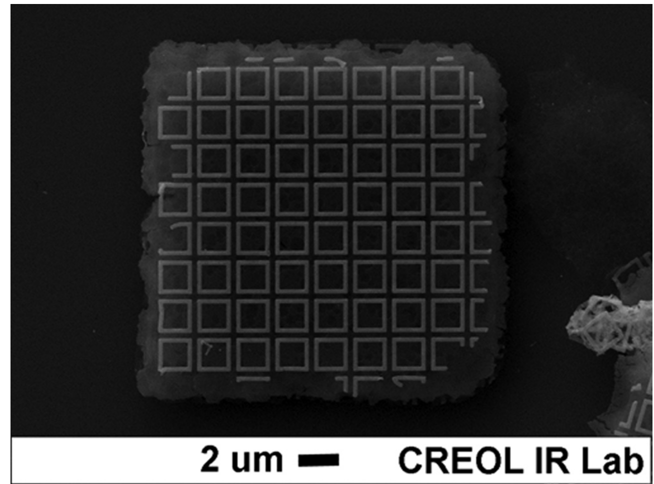

FIG. 4. SEM micrograph of single square-loop flake.

Figure 5 is an SEM image showing the cross section of a square loop-flake. Here, one can see the resonant cavity, elements, and cladding layer on either side of the Cr ground plane.

We measured wavelength-dependent reflectivity in areas with high concentrations of flakes, such as those seen in Figs. 6 and 7. Figure 6 shows a typical assortment of many flakes, while Fig. 7 shows the flakes on a scale close to that of the FTIR input aperture (100 μm diameter). The flakes tend to lie flat on the collection wafer unless they overlap; from the SEM images, we estimate that the majority of the flakes are oriented within ±15° from normal incidence. A crude estimate of the spatial fill factor of the flakes in the measurement area can be made by placing a grid over the figure to compare the flake filled sections to the voids. For Fig. 7, this yields a fill factor of approximately 65%. (As the process fabrication and collection process evolves, a more rigorous approach to distribution analysis will be developed). In Fig. 7, one can also see that a design without a guard ring results in jagged edges and a few left over Au elements, since Au is not effected by the CF_4:O_2 plasma etch.

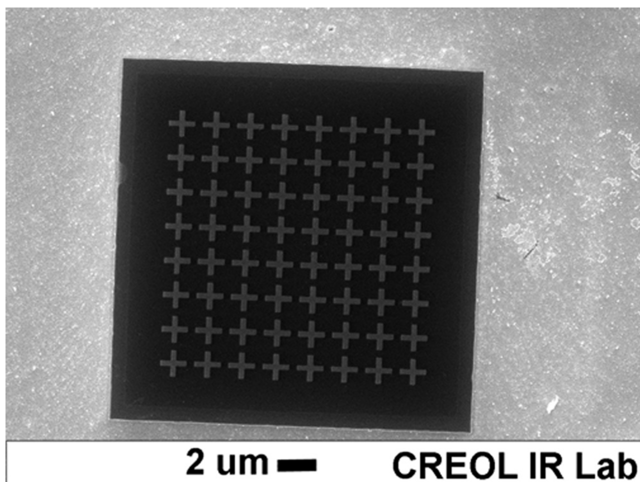

FIG. 3. SEM micrograph of single crossed-dipole flake.

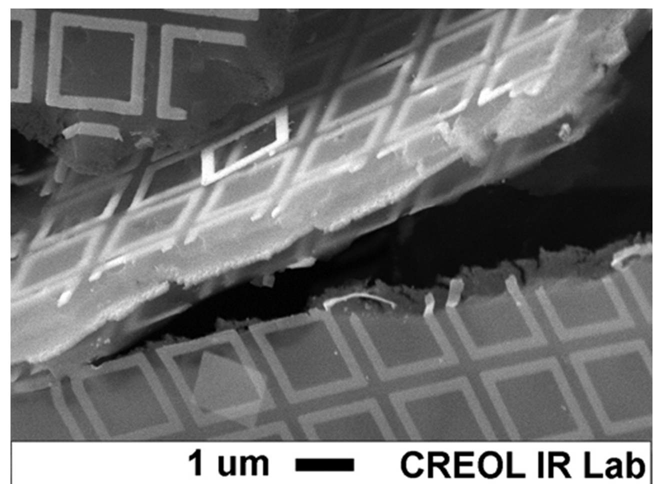

FIG. 5. SEM micrograph of the edge of a square-loop flake, showing the Au elements, BCB cavity, and Cr ground plane.

Author complimentary copy. Redistribution subject to AIP license or copyright, see http://jvb.aip.org/jvb/copyright.jsp

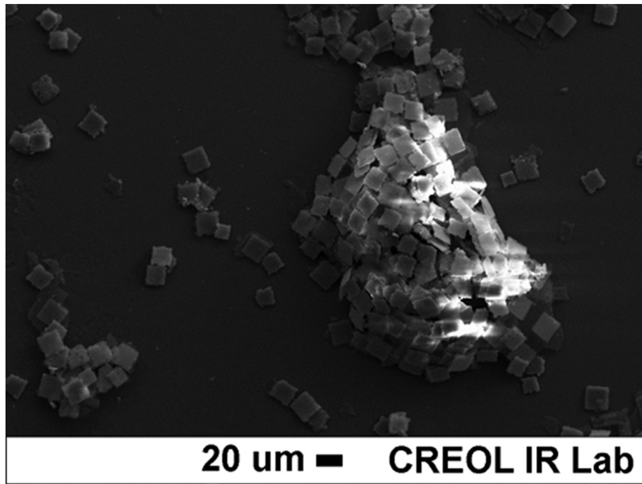

FIG. 6. SEM micrograph showing a large collection of metamaterial flakes. The whitish haze is from charging in the dielectric layer.

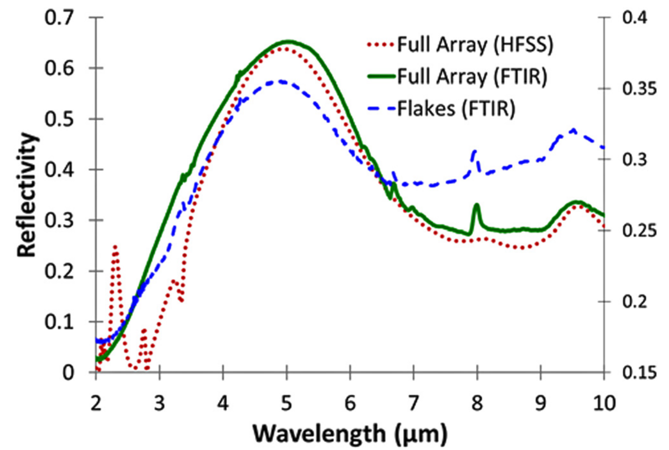

FIG. 8. (Color online) Measured reflectivity of crossed-dipole flakes (plotted on right axis) compared with the measured and simulated reflectivity of the full array (plotted on left axis).

In Fig. 8, we compare the reflectivity of collected crossed-dipole flakes to that of the full array of unit cells still on the wafer and also that which was predicted by our HFSS model (the reflectivity of the flakes is plotted on the right axis). As seen in Fig. 7, the flakes are not completely filling the input aperture of the FTIR. Additionally, the guard ring reduced the number of elements per flake, decreasing the fill factor even further. Still, the reflectivity of the flakes successfully matches the shape and modulation of the full array and simulation. Figure 9 compares the reflectivity spectra of the collected square-loop flakes to the reflectivity spectra of the full array and the reflectivity predicted by the simulation. We note again that the full array data are plotted on the left axis while the flake data are plotted on the right axis. The fill factor of our flake coating has weakened the reflectivity amplitude, while the shape of the reflectivity features has been maintained. The bands near 8 and 9.5 μm appearing in all three data sets are due to absorption peaks in the BCB. Figure 10 shows the simulated reflectivity of an infinite array of square-loop elements with respect to angle of incidence. The simulations show that the strength of resonance and modulation vary only slightly from normal incidence through 30°. In fact, major deviations of the reflectivity do not occur until 45°. Comparing Fig. 10 to Fig. 9, we infer that differences between simulated and flake reflectivity are not primarily due to the random angle of incidence of the flakes; it is more likely that any changes in spectral behavior are caused by a combination of fill factor of the measurement and the finite array dimension of the flakes.

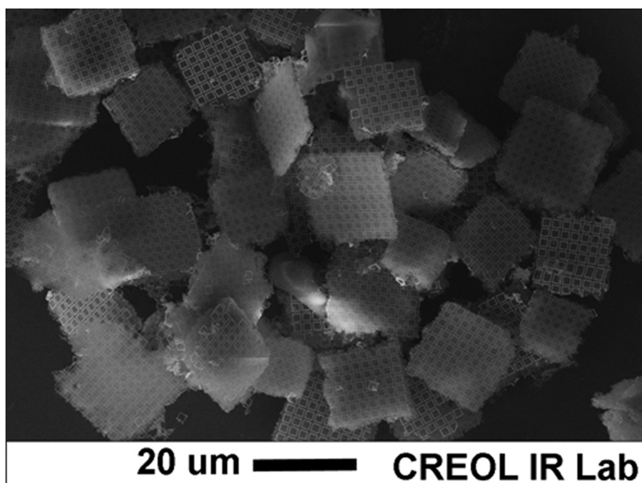

FIG. 7. SEM micrograph of an area of square loop-flakes representing the typical sample size for FTIR measurements, showing and assortment of rotational and azimuthal orientations.

V. CONCLUSIONS

We have shown, for two different designs, that infrared metamaterial elements can be incorporated into releasable flakes. Furthermore, we have shown that collections of these flakes bear a spectral signature similar to both numerical models of and measurements of the full array, when fill factor of the measuring apparatus is accounted for. In future work, we will implant these flakes within an IR-transparent binder and develop processes to optimize uniformity. In

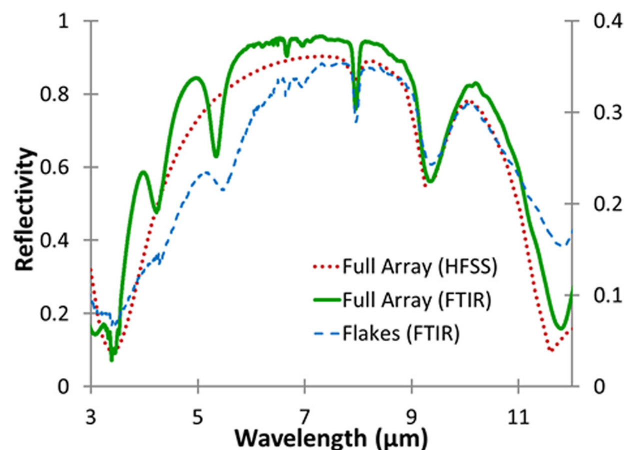

FIG. 9. (Color online) Measured reflectivity of square-loop flakes (plotted on right axis) compared with the measured and simulated reflectivity of the full array (plotted on left axis).

Author complimentary copy. Redistribution subject to AIP license or copyright, see http://jvb.aip.org/jvb/copyright.jsp

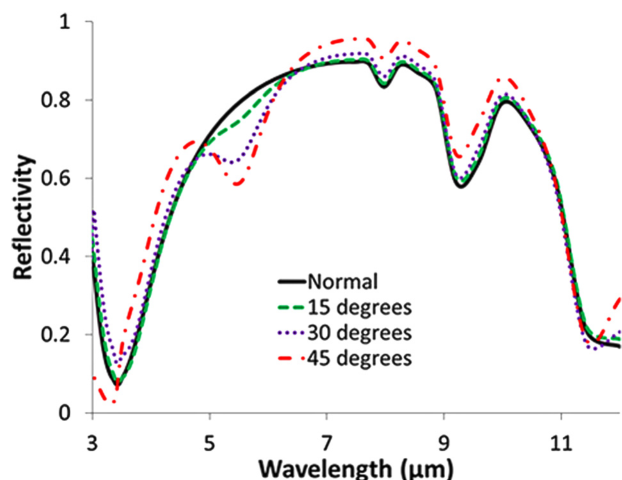

FIG. 10. (Color online) Simulated reflectivity of a full array of square-loop flakes is shown for normal incidence, 15°, 30°, and 45°.

addition, the effects of truncation of the arrays will be further investigated. We also are exploring large-scale production techniques, to lower the costs associated with serial direct-write processes.

ACKNOWLEDGMENTS

This research was supported by the Laboratory Directed Research and Development program at Sandia National Laboratories. Sandia is a multiprogram laboratory operated by Sandia Corporation, a Lockheed Martin Company, for the United States Department of Energy's National Nuclear Security Administration under Contract DE-AC04-94AL85000.

[1]D. J. Shelton, K. R. Coffey, and G. D. Boreman, Opt. Express **18**, 1330 (2010).
[2]D. H. Kwon, X. Wang, Z. Bayraktar, B. Weiner, and D. Werner, Opt. Lett. **33**, 545 (2008).
[3]Y. Avitzour, Y. A. Urzhumov, and G. Shvets, Phys. Rev. B **79**, 045131 (2009).
[4]D. J. Shelton, J. S. Tharp, G. Zummo, W. R. Folks, and G. D. Boreman, J. Vac. Sci. Technol. B **25**, 1827 (2007).
[5]H. Tao, A.C. Strikwerda, K. Fan, C.M. Bingham, W. J. Padilla, X. Zhang, and R. D. Averitt, J. Phys. D **41**, 23 (2008).
[6]X. G. Peralta, M. C. Wanke, C. L. Arrington, J. D. Williams, I. Brener, A. Strikwerda, R. D. Averitt, W. J. Padilla, E. Smirnova, A. J. Taylor, and J. F. O'Hara, Appl. Phys. Lett. **94**, 16 (2009).
[7]B. A. Munk, *Finite Antenna Arrays and FSS* (Wiley-Interscience, New York, 2003).
[8]H. Y. Yang, S. X. Gong, P. F. Zhang, F. T. Zha, and J. Ling, Microwave Opt. Technol. Lett. **51**, 10 (2009).
[9]A. Janhsen and V. Hansen, IEE Proc. H **138**, 1 (1991).
[10]J. Ginn, B. Lail, D. Shelton, J. Tharp, W. Folks, and G. Boreman, ACES J. **22**, 184 (2007).
[11]B. E. Maile, W. Henschel, H. Kurz, B. Rienks, R. Polman, and P. Kaars, Jpn. J. Appl. Phys. **39**, 6836 (2000).
[12]See: "CYCLOTENE 3000 Series Advanced Electronic Resins – Processing Procedures for CYCLOTENE 3000 Series Dry Etch Resins," 20 Oct. 2010, www.dow.com/cyclotene.

Author complimentary copy. Redistribution subject to AIP license or copyright, see http://jvb.aip.org/jvb/copyright.jsp